Mathematical Analysis of Fractal Kink-Antikink Collisions in the ϕ^4 Model

R.H. Goodman

Abstract We analyze the fractal structure seen in kink-antikink collisions of the ϕ^4 equation. The analysis is based on qualitative ODE models related to those obtained using the variational approximation. We derive a discrete-time iterated map approximation to the dynamics, from which many features of the model ODE system may be derived. We discuss the problems with Sugiyama's variational model that have been pointed out recently by Takyi and Weigel.

1 Introduction

Intriguing behavior has long been observed in the dynamics of collisions between kinks and antikinks of the ϕ^4 model

$$\phi_{tt} - \phi_{xx} - \phi + \phi^3 = 0. \tag{1}$$

This equation possesses a family of traveling-wave solutions called kinks

$$\phi(x,t) = \phi_{\mathrm{K}}(x - vt) = \tanh\left(\xi/\sqrt{2}\right)$$

where $\xi = (x - x_0 - vt)/\sqrt{1 - v^2}$ for any velocity v, $-1 < v < 1$, and another family called antikinks $\phi_{\bar{\mathrm{K}}} = -\phi_{\mathrm{K}}$.

Consider a solution described by a kink and an antikink propagating toward each other from $\pm\infty$ with equal and opposite velocities. Researchers began simulations of this situation in the 1970's. Kudryavstev and Sugiyama separately found, through

Roy H. Goodman
Department of Mathematical Sciences,
New Jersey Institute of Technology,
University Heights, Newark, NJ 07102,
e-mail: goodman@njit.edu

simulations with a small number of incident velocities, that sufficiently slow kinks and antikinks could be captured into a localized bound state [1, 2]. Ablowitz, Ladik, and Kruskal simulated a slightly larger number of initial conditions and made the surprising discovery that at one particular velocity, the kink and antikink collided, began to move apart, turned around, collided a second time, and then escaped [3]. More systematic numerical experiments by Campbell et al. showed a rich structure in the dynamics following such collisions [4, 5]. Solitary wave pairs with speed above some critical value v_c reflected off each other and escaped after colliding once. Most initial speeds below v_c led to capture: the kink and antikink form a bound state and never escape, although the localized solution subsequently decays due to the escape of radiation. However there exists a sequence of intervals such that, for initial speeds lying in such an interval, the kink and antikink collide, begin to separate, and then return to collide a second time before escaping. They called these intervals *two-bounce resonance* windows. More recent numerical simulations, e.g. [6], have shown that in between the two-bounce resonance windows are successively narrower windows where the solitary waves collide three, four, or even more times before escaping. This sensitive dependence of the output state on the input state is known as chaotic scattering [7]. These window intervals are interwoven in a manner that has been described as fractal. One such computation is shown in Figure 1. Plots of various solutions are shown in Figure 2. Careful inspection of panels (a) and (c) shows that in each successive two-bounce window, the dynamics contains one more internal oscillation than in the previous window. The initial condition in (c) was chosen to miss the peak of the resonance window, and the escaping solution is clearly more oscillatory than in panel (a).

collisions Campbell and his collaborators hypothesized that the two-bounce resonance phenomenon is due to a resonant exchange of energy between the propagating solitary waves and an internal mode, i.e. an eigenfunction corresponding to a discrete eigenvalue in the linearized operator of the ϕ^4 equation (1) about ϕ_K. The authors ran a series of numerical experiments in similar nonlinear KG systems, which allowed them to investigate this hypothesis. One such system, the double sG equation possesses a tunable parameter η. The existence/non-existence of the internal mode depends on the value of this parameter, and the authors of the paper concluded that the existence of the two-bounce resonance phenomenon depends on the internal mode.

This conclusion has, in recent years, been reversed by a group that includes Dorey, Romańczukiewicz, Shnir and collaborators [8, 9, 10], who have shown that the phenomenon exists in systems with no internal mode. This is covered in more detail in Chapter 2 of this volume.

The collective coordinates method, usually derived using the variational approximation (VA), has been the most common tool in analyzing this phenomenon. These methods go back at least to Bondeson et al. [11], and are well-described in the review article of Malomed [12]. Such methods are applied to PDEs such as (1) describing the time evolution of a spatially dependent field $\phi(x,t)$ that minimizes a Lagrangian action

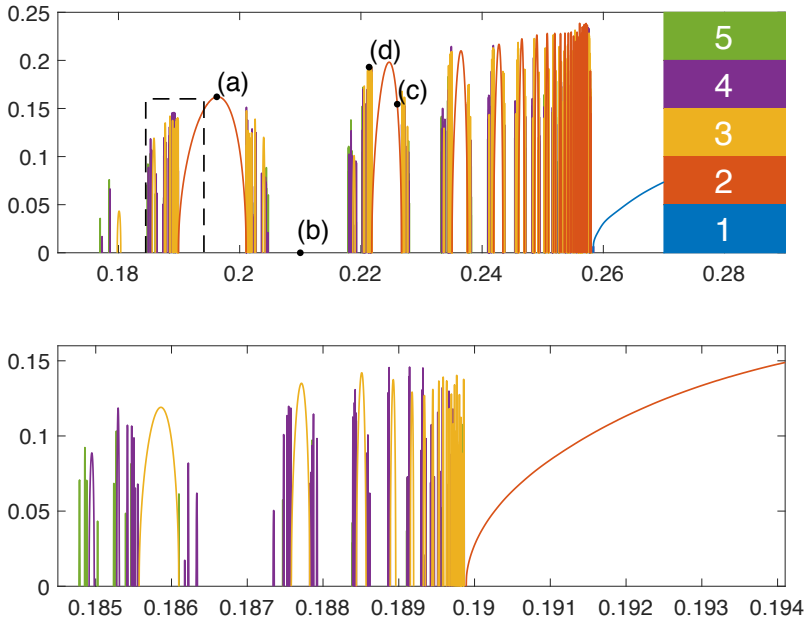

Fig. 1 (Top) The input velocity vs. the output velocity, showing solutions that escaped after five or fewer collisions. Other initial conditions either led to capture or to escape after more than five collisions. (Bottom) Magnification of the interval indicated by the dashed line in the top image.

$$\mathcal{A} = \iint \mathcal{L}(\phi) dx\, dt.$$

Instead of minimizing the action over all functions ϕ in the appropriate space, one chooses a solution ansatz dependent on a finite number of time-dependent parameters and minimizes the Lagrangian over all functions in that finite-dimensional family of functions. After integrating out the spatial dependence, one arrives at a finite-dimensional Lagrangian, whose Euler-Lagrange equations describe the evolution of the parameters. It is common to neglect higher-order terms that appear in this approximation.

A variational model was derived for the kink-antikink collision by Sugiyama in 1979 [2], and was later studied by Anninos et al. [13]. We presented a thorough analysis of this model in 2005, which we thought, together with some followups, would close the books on this problem [6, 14, 15].

Recent work by Weigel and his students has cast doubt on the validity of the VA models [16, 17]; this is covered in more detail in Chapter 3 of this volume, so the account here will be brief. There are two main issues. The first, initially noted by Caputo and Flytzanis [18] is that the mass matrix for the VA equations is singular at the instant the kink and antikink collide. An attempt to remedy this is discussed in Ref. [16]. The second is a mistake in the form of the term coupling the traveling wave to the internal mode in the VA approximation derived by Sugiyama and used, without correction in many subsequent studies, including [6]. Most damningly, they show

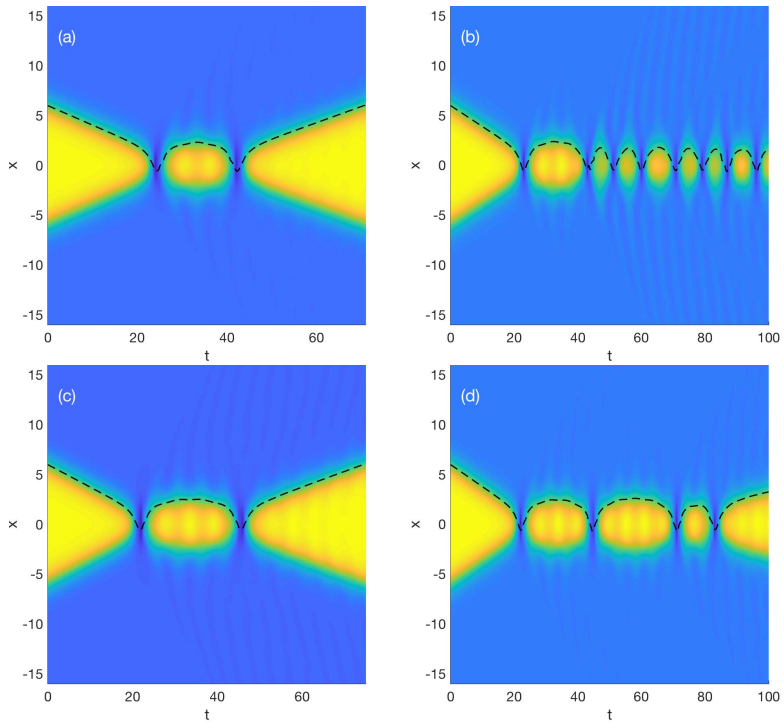

Fig. 2 Kink-antikink solutions to the ϕ^4 equation, with initial velocities demonstrating (a,c) two bounces, (b) capture, and (d) three bounces, corresponding to marked points in Fig. 1.

that replacing the incorrect term with its correct value further degrades the agreement between the full system and its VA model. They then show that the inclusion of higher-order terms ignored by Sugiyama, far from improving the model's agreement with PDE simulations, leads to additional disagreement, both quantitative and qualitative.

In addition, the inadequacy of the model equations has long been apparent due to the energy conservation. While the ϕ^4 equation conserves energy, the total energy available to the solitary waves after they collide is reduced by the propagation of radiation away from the location of the collision, as is clearly visible in Fig. 2 as ripples in the blue region emanating from the location of the collision. As a result of this energy loss, the outgoing velocity of the escaping solitons shown in Fig. 1 is never more than about ninety percent of that of the incoming soliton. By contrast, there is no radiative mode to carry energy away in the collective-coordinate model derived via the VA method. The condition used to define the resonant initial velocities is that the incoming and outgoing speeds are precisely equal. Clearly if energy loss due to radiation plays such a large role, then correct the form of the conservative collective coordinates model will be insufficient to account for its role.

2 Analysis of collective-coordinate models

Work described in the previous section and elsewhere in this volume casts serious doubt on the correctness of the collective coordinates model derived by Sugiyama and analyzed by Goodman and Haberman. Nonetheless, in some cases the variational models have been quite effective in reproducing dynamics seen in the PDE from which they were derived. For example, Fei et al. derived a collective coordinate model that describes the behavior of solitons colliding with localized defects in the medium through which they propagate [19]. As in the case for the ϕ^4 equation, the approximations used in deriving the reduced model are unjustified and probably unjustifiable.

However the models derived by VA are important as phenomenological models. They distill an essential feature of such systems: the interaction between the kink and antikink is well described by a localized potential that decays at infinity, and the interaction between a kink and its internal mode is mediated by the presence of a nearby antikink. Therefore analyzing such models can provide insight into the dynamics of collisions even if the model equations do not describe the full dynamics in the sense of a convergent approximation.

2.1 The ODE Model

Sugiyama's VA model is derived using the ansatz

$$\phi_{\text{ansatz}}(x,t) = \phi_{\text{K}}(x + X(t)) - \phi_{\text{K}}(x - X(t)) + 1 + A(t)\big(\chi_1(x + X(t)) - \chi_1(x - X(t))\big),$$

where $X(t)$ is the undetermined position of the kink and $-X(t)$ that of the antikink, with the internal modes at the same location and with amplitude $A(t)$. The internal mode has the form

$$\chi_1(\xi) = \left(\frac{3}{\sqrt{2}}\right)^{1/2} \tanh\xi \,\operatorname{sech}\xi.$$

The resulting system has a mass matrix that depends on the position $X(t)$, and which is singular at $X = 0$, when the kink and antikink profiles cancel each other exactly. We present a qualitative model that retains the essential features of such a model while avoiding this difficulty [14, 15, 20]. It consists of a system of second order ODE

$$m\ddot{X} + U'(X) + \epsilon F'(X)A = 0; \tag{2a}$$

$$\ddot{A} + \omega^2 A + \epsilon F(X) = 0. \tag{2b}$$

This conserves an energy

$$H = \frac{m}{2}\dot{X}^2 + U(X) + \frac{1}{2}(\dot{A}^2 + \omega^2 A^2) + \epsilon F(X)A. \tag{3}$$

It is assumed that the potential $U(X)$ and the coupling function $F(X)$ decay rapidly as $X \to \infty$ and that $U(X)$ grows rapidly with negative X to prevent the waves from passing through each other. The other essential ingredient is that $U(X)$ has a minimum, so that, when uncoupled from the secondary oscillator A, the kink and antikink may oscillate around this minimum and be trapped, or, if they have sufficient energy, escape to infinity. Between these two regimes lies the *separatrix* curve, which is an orbit homoclinic to the point at infinity. We will let $U(X)$ be the Morse potential and $F(X)$ be a simple decaying exponential:

$$U(X) = e^{-2X} - e^{-X};\ F(X) = e^{-X}. \tag{4}$$

Setting $\epsilon = 0$ decouples the dynamics, with X conserving an energy $E = \frac{m}{2}\dot{X}^2 + U(X)$. The phase plane for this system is plotted in Figure 3. The separatrix corresponds to the level set $E = 0$ and to trapped orbits to negative energy. Also plotted in this figure is the projection into the $(X, \dot{X})$ plane of one solution to the equations with $\epsilon = \frac{1}{4}$.

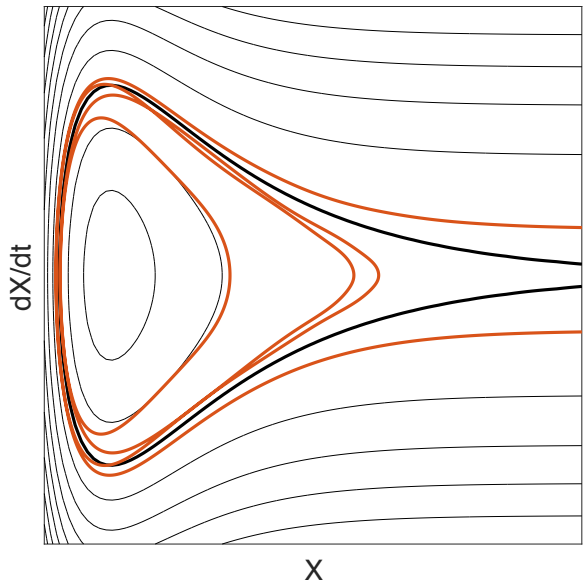

Fig. 3 The $(X, \dot{X})$ phase plane, and the projection of a solution to system (2) that begins in the lower-right-hand corner, crosses to the inside of the separatrix, makes four bounces, and then crosses out again at the upper-right.

Figure 4(a) shows the result of solutions to the model ODE system with initial conditions

$$X(0) = X_{\max} \gg 1;\ \dot{X}(0) = -v_{\text{in}};\ a(0) = 0;\ \dot{a}(0) = 0$$

with 50,001 evenly-spaced spaced values of v_{in} and parameters $m = 1$, $\omega = 1$, and $\epsilon = \frac{1}{4}$. The color indicates how many collisions, i.e. minima of $X(t)$ occurred before escape, determined by $X(t) > X_{\text{max}}$. True capture is possible for the ϕ^4 system, as evidenced by figure 1(d). In these cases energy that escapes to infinity in the form of radiation prevents the solitary waves from escaping. By contrast, in the model ODE system (2), eventually, enough energy must be returned to the propagating mode $X(t)$ for it to escape, except for a measure-zero set of initial conditions that lie on the stable manifold of a bounded orbit. Therefore, capture is not observable in this figure. Note that this figure captures much of the structure of the PDE computation, although not the quantitative details.

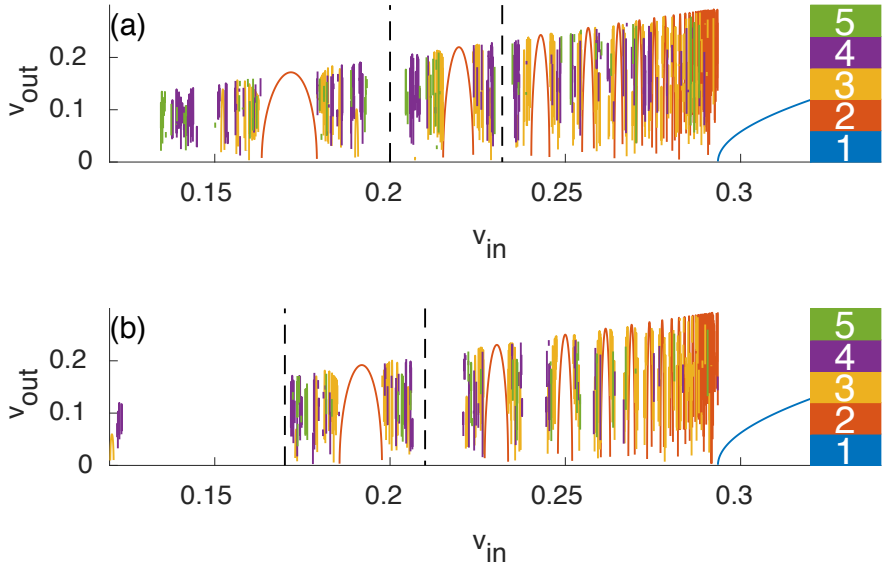

Fig. 4 (a) Numerical simulation of chaotic scattering in the model ODE system (2) with parameters $m = 1$, $\omega = 1$, and $\epsilon = \frac{1}{4}$. (b) Numerical simulation of the iterated map model (10).

2.2 Derivation of the discrete-map approximation

The chaotic scattering is analyzed by deriving a discrete map approximation to the dynamics. Referencing Figure 5, we see that $X(t)$ approaches $-\infty$ as $t \to \infty$, achieves a local minima at a discrete sequence of "bounce " times t_j, and following the last minimum, at $t = t_4$, escapes. Also defined are the times $\tilde{t}_j$ at which the solitary waves achieve their largest separations. By definition $\tilde{t}_0 = \infty$ and the final separation time $\tilde{t}_4 = \infty$. The second panel shows the energy $E(t)$ in the $(X, \dot{X})$ component, which is positive when the solution is outside the separatrix, and which jumps at

each bounce. The third panel shows that $a(t)$ oscillates sinusoidally, with a jump in amplitude and phase at each bounce. The map we derive measures how the energy E, and the amplitude and phase of a change between the bounces.

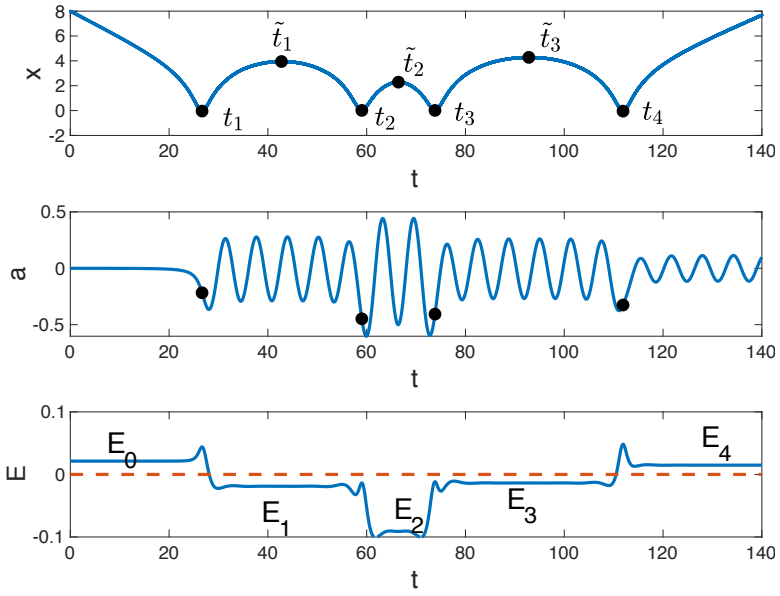

Fig. 5 The solution to equation (2) plotted in Fig. 3. Top: $X(t)$, showing the four bounce times and three near-infinity approach times. Middle: $a(t)$ showing that the amplitude and phase of the oscillator a change at each bounce. Bottom: The energy, which is positive when the solution is outside the separatrix, and negative inside.

Rather than describing $a(t)$ by the amplitude and phase, we instead assume that before bounce j,

$$A(t) \sim C\left(c_j \cos\omega(t-t_j) + s_j \sin\omega(t-t_j)\right) \text{ as } t - t_j \to -\infty$$

where the constant C must be chosen to normalize the variables (see below). This represents the value of $a(t)$ when X is large and the coupling is smallest. The map we derive takes the form

$$(c_{j+1}, s_{j+1}, E_{j+1}) = \mathcal{F}(c_j, s_j, E_j)$$

where E_j is the plateau energy level preceding the jth bounce time t_j.

Near time t_j, $X(t)$ can be represented by the solution along the separatrix $X_S(t-t_j)$, and we can solve equation (2b) for $A(t)$ by variation of parameters:

$$\begin{aligned} A(t) \sim & C\left(c_j \cos\omega(t-t_j) + s_j \sin\omega(t-t_j)\right) \\ & - \frac{\epsilon}{\omega}\sin\omega(t-t_j)\int_{-\infty}^{t} F(X_S(t-t_j))\cos\omega(t-t_j)dt \\ & + \frac{\epsilon}{\omega}\cos\omega(t-t_j)\int_{-\infty}^{t} F(X_S(t-t_j))\sin\omega(t-t_j)dt \end{aligned} \tag{5}$$

Since X_S is an even function of t, this gives, as $t - t_j \to \infty$,

$$\begin{aligned} A(t) \sim & C\left(c_j \cos\omega(t-t_j) + s_j \sin\omega(t-t_j)\right) \\ & - \frac{\epsilon}{\omega}\sin\omega(t-t_j)\int_{-\infty}^{\infty} F(X_S(t-t_j))\cos\omega(t-t_j)dt \end{aligned}$$

Defining

$$C = \frac{\epsilon}{\omega}\int_{-\infty}^{\infty} F(X_S(t))\cos\omega t dt = \frac{\epsilon}{\omega}\int_{-\infty}^{\infty} F(X_S(t))e^{i\omega t}dt, \tag{6}$$

we may rewrite this as

$$A(t) \sim C\left(c_j \cos\omega(t-t_j) + (s_j - 1)\sin\omega(t-t_j)\right) \text{ as } t - t_j \to \infty.$$

However, this should be written instead in terms of $t - t_{j+1}$. Note that the value of C is the first instance in this calculation where the particular form of the coupling function $F(X)$ is important.

Letting $\theta_{j+1} = -\omega(t_{j+1} - t_j)$, then $\omega(t - t_j) = \omega(t - t_{j+1}) - \theta_{j+1}$ and using angle addition formulas, we arrive at

$$A(t) \sim C\left(c_{j+1}\cos\omega(t-t_{j+1}) + s_{j+1}\sin\omega(t-t_{j+1})\right),$$

where

$$\begin{pmatrix} c_{j+1} \\ s_{j+1} \end{pmatrix} = \begin{pmatrix} \cos\theta_{j+1} & -\sin\theta_{j+1} \\ \sin\theta_{j+1} & \cos\theta_{j+1} \end{pmatrix}\begin{pmatrix} c_j \\ s_j - 1 \end{pmatrix}.$$

We introduce a complex variable $z_j = c_j + is_j$, which renders this as

$$z_{j+1} = e^{i\theta_{j+1}}\left(z_j - i\right). \tag{7}$$

Now it remains to approximate $(t_{j+1} - t_j)$. This requires matching a solution in a neighborhood of the bounce, where $X(t)$ is approximated by the separatrix orbit, with the solution near $X = \infty$. Here the leading-order behavior of $U(X)$ for large X is sufficient to describe the dynamics. The most important quantity for describing the large-X behavior is the energy in the X-component of the solutions

$$E = \frac{m}{2}\dot{X}^2 + U(X).$$

The time $t_{j+1} - t_j$ is related to the energy on the j^{th} approach to infinity, so we must calculate how the energy changes. To do so, we integrate $\frac{dE}{dt}$ between the two

near-infinity approach times. The trajectory is assumed to be in a neighborhood of the separatrix, so that the collision times are far apart, and the domain of integration can be replaced by $(-\infty, \infty)$. An integral of this type is known as a *Melnikov integral* [21].

$$E_{j+1} - E_j = \int_{\tilde{t}_{j-1}}^{\tilde{t}_j} \frac{dE}{dt} dt \approx \int_{-\infty}^{\infty} \frac{dE}{dt} dt$$
$$= \int_{-\infty}^{\infty} \left(\ddot{X} + U'(X)\right) \dot{X} dt = \int_{-\infty}^{\infty} -\epsilon A F'(X) \dot{X}\, dt = \epsilon \int_{-\infty}^{\infty} F(X) \dot{A}\, dt,$$

and the integration by parts is justified since $F(X(t))$ vanishes sufficiently rapidly as $|t \to \infty|$.

In the above calculation, the only assumption so far is that the domain of integration can be approximated by the whole line, so the integrand must vanish sufficiently rapidly as $|t \to \infty|$. We further approximate $X(t)$ in the last expression by $X_S(t - t_j)$. The rest of the calculation depends on the specific form of functions $F(X)$ and $U(X)$ in the Hamiltonian (3). For the particular form of $U(X)$ specified in equation (4), the separatrix orbit is $X_S(t) = \log\left(1 + \frac{t^2}{2m}\right)$ and $F(X_S) = \frac{2m}{2m+t^2}$.

Using this form for $F(X)$, calculating $\dot{A}$ using equation (5), and integrating, taking advantage of symmetries, we arrive at

$$E_{j+1} - E_j = \frac{C^2\omega^2}{2} \left(2s_j - 1\right). \tag{8}$$

We define a rescaled energy by $E_j = \frac{C^2\omega^2}{2} \mathcal{E}_j$. Equations (7) and (8) then imply the conservation of the quantity

$$\mathcal{H} = \mathcal{E}_j + \left|z_j\right|^2 \tag{9}$$

A delicate matching procedure that depends on $U(X)$ is needed to determine the functional form of $\theta_{j+1} = \Theta(\mathcal{E}_{j+1})$. Using equation (7) and the conservation law (9), the map becomes

$$z_{j+1} = e^{i\Theta(\mathcal{H} - |z_j - i|^2)}(z_j - i).$$

The integral (6) may be evaluated by residues and yields

$$C = \frac{\epsilon\pi\sqrt{2m}}{\omega} e^{-\sqrt{2m}\omega}.$$

When $E_{j+1} < 0$, the time between bounces $t_{j+1} - t_j$ can be calculated via a matched asymptotic procedure between the near-saddle approaches, described by the separatrix orbit and the near-infinity approaches defined using the large X asymptotic expansion of $U(X)$, following [15]. Since the phase of θ_{j+1} enters the computation, it is necessary to approximate this quantity to $o(1)$. For this potential $U(X)$ given by (4), the time $(t_{j+1} - t_j)$ is simply the period of an orbit with energy $E_{j+1} < 0$, yielding

$$\Theta(\mathcal{E}_j) = -\frac{2\pi}{C}\sqrt{\frac{m}{-\mathcal{E}_j}}.$$

Finally, following Stolovitsky et al. [22], we define a new variable

$$Z_j = z_j - \frac{i}{2}$$

and a parameter $\alpha = 2\pi\sqrt{M}/C = \sqrt{2}\omega e^{2m\omega}/\epsilon$. With respect to this coordinate, the final form of the *separatrix map* is

$$\mathcal{F}(Z_j) = e^{-i\alpha/\sqrt{|Z_j - \frac{i}{2}|^2 - \mathcal{H}}}\left(Z_j - \frac{i}{2}\right) - \frac{i}{2}, \tag{10}$$

with inverse

$$\mathcal{F}^{-1}(Z_j) = e^{i\alpha/\sqrt{|Z_j + \frac{i}{2}|^2 - \mathcal{H}}}\left(Z_j + \frac{i}{2}\right) + \frac{i}{2}.$$

Despite being written in terms of a complex variable, these maps are non analytic as they involve absolute values. Defining ρ to be the complex conjugation operator $\rho(z) = z^*$, the two maps are related by conjugation,

$$\mathcal{F}^{-1} = \rho^{-1}\mathcal{F}\rho.$$

2.3 Interpretation and analysis of the map

The traditional set of tools may be applied to the map (10) such as the enumeration of fixed points, period-n points, and stable and unstable manifolds. Much of this is done in Ref. [15]. Here we concentrate on using the map to explain the structure found in Figure 4. Each point in this figure corresponds to a different initial velocity, and thus a different value of $\mathcal{H}$, and a different map, so computing such quantities does not seem to be the most useful calculation.

For $\mathcal{H} > 0$, the domain of $\mathcal{F}$ excludes the closed disk

$$\mathcal{D}_{\text{out}} = \left\{Z : \left|Z - \frac{i}{2}\right| \leq \mathcal{H}\right\}.$$

Its range, and the domain of $\mathcal{F}^{-1}$ is the complex plane excluding the closed disk

$$\mathcal{D}_{\text{in}} = \left\{Z : \left|Z + \frac{i}{2}\right| \leq \mathcal{H}\right\}.$$

The two disks are shown in Figure 6. These sets have an important and simple interpretation for the dynamics. For $Z_j \in \mathcal{D}_{\text{out}}$, $\mathcal{E}_{j+1} > 0$ is well-defined, but t_{j+1} is not, because solutions with positive energy escape to infinity and there is no $(j+1)th$

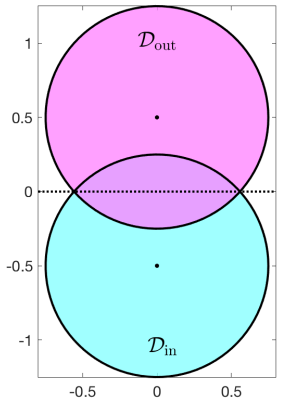

Fig. 6 The two disks on which the map $\mathcal{F}$ and its inverse are undefined. On the intersection, neither is defined.

bounce. Similarly points in $\mathcal{D}_{\text{in}}$ have no pre-image under the map and correspond to kink-antikink pairs arriving from infinity.

We assume that the internal mode is initially unexcited, i.e. $c_0 = s_0 = 0$ or to $Z_0 = -\frac{i}{2}$, the point at the center of the disk $\mathcal{D}_{\text{in}}$. If $\mathcal{H}$ is sufficiently large, then the point $Z_0 = -\frac{i}{2} \in \mathcal{D}_{\text{out}}$ and the solitary waves escape each other's embrace after just on interaction. Therefore the critical velocity is that such that $\mathcal{H}|_{v=v_c} = 1$, i.e. that

$$\mathcal{H}(v_c) = \mathcal{E} = \frac{2}{\omega^2 C^2} E = \frac{2}{\omega^2 C^2} \cdot \frac{m v_c^2}{2},$$

or

$$v_c = \frac{\omega C}{\sqrt{m}}. \tag{11}$$

This gives a useful relation

$$\mathcal{H} = \frac{v^2}{v_c^2}. \tag{12}$$

We will illustrate two features of this dynamics: the n-bounce resonant solutions and the hierarchy of the resonance windows. The n-bounce resonant solutions satisfy $Z_0 = -\frac{i}{2}$ and $Z_{n-1} = \frac{i}{2}$,

$$\mathcal{F}^{n-1}\left(-\frac{i}{2}\right) = \frac{i}{2}$$

if $n = 2m$ is even then

$$\mathcal{F}^m\left(-\frac{i}{2}\right) = \mathcal{F}^{-(m-1)}\left(\frac{i}{2}\right) = \rho \mathcal{F}^{(m-1)}\left(-\frac{i}{2}\right),$$

i.e.

$$\mathcal{F}(Z_m) = Z_m^*. \tag{13}$$

If $n = 2m + 1$ is odd then

$$\mathcal{F}^m\left(-\frac{i}{2}\right) = \mathcal{F}^{-m}\left(\frac{i}{2}\right) = \rho\mathcal{F}^m\left(-\frac{i}{2}\right),$$

i.e.

$$Z_m \in \mathbb{R}. \tag{14}$$

The edges of the n-bounce resonance windows correspond to the points that land on the boundary of the disk $\mathcal{D}_{\text{out}}$ after $n - 1$ iterates, i.e. those for which

$$\left|Z_{n-1} - \frac{i}{2}\right|^2 = \mathcal{H}. \tag{15}$$

Given $Z_0 = -\frac{i}{2}$, then

$$Z_1 = -ie^{-i\phi_1} - \frac{i}{2} \text{ and } Z_2 = -ie^{-i\phi_2}\left(e^{-i\phi_1} + 1\right) - \frac{i}{2},$$

where

$$\phi_1 = \frac{\alpha}{\sqrt{1-\mathcal{H}}} = \frac{2\pi\omega}{\sqrt{v_c^2 - v^2}} \text{ and } \phi_2 = \frac{\alpha}{\sqrt{4\cos^2\frac{\phi_1}{2} - \mathcal{H}}} = \frac{2\pi\omega}{\sqrt{4v_c^2\cos^2\frac{\pi\omega}{\sqrt{v_c^2-v^2}} - v^2}}.$$

These have all been put into a form where the dependence of the solution on the initial velocity v has been made explicit.

The condition for a two-bounce resonant initial velocity (13) is then just $Z_1 = i$, which can be simplified to $e^{i\phi_1} = -1$, or

$$v_{2,n} = \sqrt{v_c^2 - \frac{4\omega^2}{(2n-1)^2}}. \tag{16a}$$

Since ϕ_1 diverges as $v \nearrow v_c$, there is an infinite number of such solutions, indexed by n, which here specifies the number of oscillations of the secondary oscillator $A(t)$ between the two collisions. This formula indicates that such a solution only exists for

$$n > \frac{1}{2}\left(\frac{2\omega}{v_c} + 1\right).$$

The edges of the two-bounce windows satisfy equation (15) with $n = 2$ which can be simplified to

$$v^2 = 4v_c^2\cos^2\frac{\pi\omega}{\sqrt{v_c^2 - v^2}}.$$

The three-bounce resonant solutions solve equation (14) with $m = 1$, i.e. that $Z_1 \in \mathbb{R}$. This can be simplified to $\cos\phi_1 = \frac{-1}{2}$, or

$$v_{3,n\pm} = \sqrt{v_c^2 - \frac{4\omega^2}{\left(2n - 1 \pm \frac{1}{3}\right)^2}}. \tag{16b}$$

Again, there is an infinite number of such solutions, immediately to the right and left of each two-bounce window. The edges of the three-bounce windows satisfy equation (15) with $n = 3$, which can be simplified to

$$v^2 = \left(1 + 8\cos\frac{\phi_1}{2}\cos\frac{\phi_2}{2}\cos\frac{\phi_1 + \phi_2}{2}\right)v_c^2.$$

Since $\phi_2 \to \infty$ as v approaches the edge of each two-bounce window, there must be an infinite number of three bounce windows accumulating outside of each two-bounce window.

We find the four-bounce resonant solutions using equation (13) with $m = 2$. This is more simply written as $e^{i(\phi_1+\phi_2)} = -1$ or

$$\phi_1 + \phi_2 = (2n - 1)\pi, \tag{16c}$$

but of course we can expand the LHS as a function of v. The five-bounce resonant solutions solve equation (14) with $n = 2$, which requires

$$\cos\phi_2 + \cos(\phi_1 + \phi_2) = -\frac{1}{2}. \tag{16d}$$

Here again, the divergence of ϕ_2 guarantees that there is an infinite number of four- and five-bounce resonant solutions. With a little bit more work we can show that an infinite sequence of $n+1$-bounce windows accumulates at the left and right edges of each n-bounce resonance. However, beyond this point, it becomes difficult to develop such explicit formulas.

3 Computational exploration of map (10)

Figure 4(b) shows the chaotic scattering diagram for solutions to the map (10) with initial condition $Z_0 = -\frac{i}{2}$. It is impossible to resolve this figure, since the angle $\Theta(Z_j)$ diverges as Z_j approaches the boundary of its domain, i.e. the circle $\partial\mathcal{D}_{\text{out}}$, which implies that the full diagram consists of an infinite number of windows of infinitesimal width.

In this figure, equation (12) is used to replace the asymptotic value of the critical velocity (11) by the numerical value obtained from numerical simulation of the ODE model ($v_c \approx 0.294$ from simulation of (2), while formula (11) gives $v_c \approx 0.279$). Numerical comparisons in Ref. [14] show that as $\epsilon \to 0$ (or as $\omega \to \infty$) the accuracy of the formula (11), and the positions of the map's predictions for resonance windows improves. However, we elect to use a relatively large value of ϵ in this figure, as the

window widths are smaller for small ϵ and it is harder for a reader to visualize the intricate structure.

In Figure 7, we show three zoomed-in views of the ODE simulation shown in Figure 4(a), with each figure showing the input velocities between the dashed black lines in the previous figure. Surrounding each n-bounce window, we can see a sequence of $(n+1)$-bounce windows, accumulating at its edges. These windows have a clearly visible envelope, including a "tallest" window which may have a resonant solution at its center. It is impossible to tell from the ODE simulations whether these are truly resonances. The best we can do is to find the input velocities which locally minimize $v_{\text{in}} - v_{\text{out}}$.

An analogous set of zooms is shown for the map (10) in Figure 8, zooming in beginning between the dashed vertical lines in Figure 4(b). For the map, the conditions (13) and (14), or more specifically equations (16) demonstrate which of the apparent n-bounce resonant velocities are and which are not actual resonances. In subplot (a), a two-bounce solution satisfying equation (16a) is flanked by two three-bounce solutions satisfying equation (16b). In subplot (b) a non-resonant three-bounce window has four-bounce windows on both sides, but the only four-bounce window satisfying condition (16c) is on its right. Subplot (c) shows two four bounce windows, each surrounded by five bounce windows, but the only five bounce window satisfying equation (16d) is to the left of a non-resonant four-bounce window.

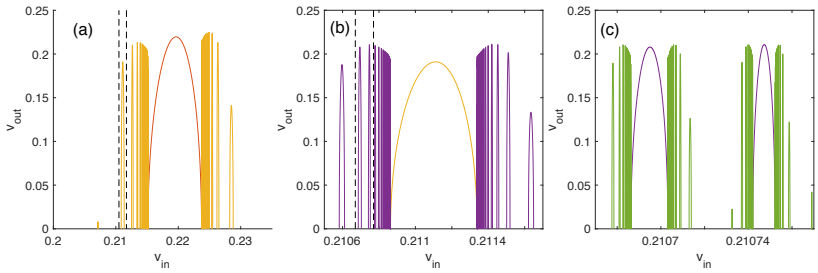

Fig. 7 Three zooms of the ODE simulation shown in Figure 4(a). From the figure it is not possible to determine which of the windows contains a resonance.

4 Conclusions and outlook

To conclude, the assumptions underlying the derivation of model ODE systems like (2) have been shown, and their numerical infidelity to the underlying PDE system has likewise been highlighted. Nonetheless, as qualitative models, they can be used to guide thinking about the types of behaviors seen in solitary wave collisions. These models are amenable to a deep analysis that allows for the explanation of many of the features seen in numerical simulations.

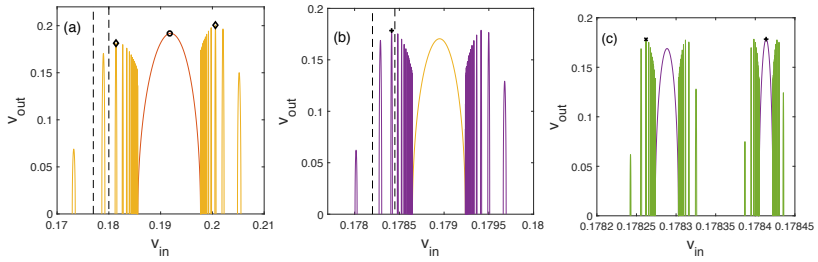

Fig. 8 Three zooms of the map simulation shown in Figure 4(b). The marked points indicate resonant solutions as determined by equations (16). Several of the points that appear to be resonances in this figure can be rejected as resonances by calculating that the quantities appearing on the LHS of the equations (16) are nonzero, indeed not close to zero.

Clearly a collective coordinates model that more completely captures the dynamics of the full PDE will be needed. Such a model should capture at least some of the energy lost due to radiation and will, ideally, be amenable to analysis like that presented here. An interesting twist is that the map will no longer obey a conserved quantity as in equation (9), and thus not be reducible from three dimensions to two. An ODE model was derived to include radiative dissipation in the interaction between sG solitons and localized defects in Ref. [23]. However the additional terms did not allow us to extend the analytic methods described in the present chapter.

Acknowledgements Many of the results in this chapter were obtained in collaboration with Dr. Richard Haberman and funded by the NSF under grants DMS-0204881, DMS-0506495, and DMS-0807284.

References

1. A.E. Kudryavtsev, JETP Lett. **22**, 82 (1975)
2. T. Sugiyama, Prog. Theor. Phys. **61**, 1550 (1979)
3. M.J. Ablowitz, M. Kruskal, J. Ladik, SIAM J. Appl. Math. **36**, 428 (1979)
4. D.K. Campbell, J.F. Schonfeld, C.A. Wingate, Physica D **9**, 1 (1983)
5. D.K. Campbell, M. Peyrard, Physica D **18**, 47 (1986)
6. R.H. Goodman, R. Haberman, SIAM J. Appl. Dyn. Sys. **4**, 1195 (2005)
7. E. Ott, T. Tél, Chaos **3**, 417 (1993)
8. P. Dorey, K. Mersh, T. Romanczukiewicz, Y. Shnir, Phys. Rev. Lett. **107**, 091602 (2011)
9. P. Dorey, T. Romanczukiewicz, Phys. Lett. B **779**, 117 (2018)
10. A. Halavanau, T. Romanczukiewicz, Y. Shnir, Phys. Rev. D **86**, 085027 (2012)
11. A. Bondeson, M. Lisak, D. Anderson, Phys. Scripta **20**, 479 (1979)
12. B.A. Malomed, Prog. Opt. **43**, 71 (2002)
13. P. Anninos, S. Oliveira, R. Matzner, Phys. Rev. D **44**, 1147 (1991)
14. R.H. Goodman, R. Haberman, Phys. Rev. Lett. **98**, 104103 (2007)
15. R.H. Goodman, Chaos **18**, 023113 (2008)
16. I. Takyi, H. Weigel, Phys. Rev. D **94**, 085008 (2016)
17. H. Weigel, J. Phys.: Conf. Ser. **482**, 012045 (2014)
18. J.G. Caputo, N. Flytzanis, Phys. Rev. A **44**, 6219 (1991)

19. Z. Fei, Y.S. Kivshar, L. Vázquez, Phys. Rev. A **45**, 6019 (1992)
20. R.H. Goodman, A. Rahman, M.J. Bellanich, C.N. Morrison, Chaos **25**, 043109 (2015)
21. G. Zaslavsky, *The Physics of Chaos in Hamiltonian Systems* (Imperial College Press, London, 2007)
22. G. Stolovitzky, T.J. Kaper, L. Sirovich, Chaos **5**, 671 (1995)
23. R.H. Goodman, P.J. Holmes, M.I. Weinstein, Physica D **161**, 21 (2002)